Simulated Biosorption of Cr^{6+} Using Peels of *Litchi chinensis sonn* by Aspen Adsorption® V8.4

Aileen D. Nieva, Ronnel C. Garcia, and Ren Mikhail R. Ped

***Abstract*—This study focuses on the investigation of the performance of *Litchi chinensis sonn* peels in a simulated fixed bed column in sequestering Cr(VI) by breakthrough curve analysis using Aspen Adsorption® V8.4. The breakthrough curve analysis was conducted by: 1) varying initial concentration at a constant flow rate and constant bed height, 2) varying flow rate at a constant initial concentration and constant bed height, and 3) varying bed height at constant flow rate and constant initial concentration. The good adsorption capacity was implied by a longer breakthrough time so as to make use of the peels of *Litchi chinensis sonn* for a longer period of time before there was a need to replace or to regenerate. Increasing the volumetric flow rate at constant initial sorbate concentration and bed height increased the breakthrough time. Increasing the initial sorbate concentration at constant volumetric flow rate and bed height decreased the breakthrough time. Increasing the bed height at a constant volumetric flow rate and initial sorbate concentration increased the breakthrough time. Longer breakthrough time denotes a better adsorption capacity. The longest breakthrough time was 335 s with volumetric flowrate at $1x10^{-3}$ L s^{-1}, initial sorbate concentration at 20 mg L^{-1}, and a bed height of 0.7 m. The shortest was 6.63 s with a volumetric flow rate at $1x10^{-2}$ L s^{-1}, initial sorbate concentration at 200 mg L^{-1}, and a bed height of 0.2m.**

***Index Terms*—Adsorption capacity, Aspen Adsorption®, breakthrough curve analysis, *Litchi chinensis sonn*.**

I. Introduction

Cr(VI) is a carcinogenic and mutagenic form of chromium, while Cr(III) is an essential element for human nutrition although the latter may be converted to Cr(VI) once ingested into the body through physiological processes. Sources of these heavy metals include industrial discharges from steel production, metal coating, dyes and pigments, leather tanning and wood preservation. Some of the reported chronic effects of this heavy metal exposure include contact dermatitis, skin ulcers, irritation and ulceration of the nasal mucosa, perforation of the nasal septum, epigastric nausea, vomiting and severe diarrhea [1]. Removal of Cr(VI) from wastewater by various methods involve high capital and operational costs. In the past decade, the use of biosorbent materials, such as agricultural wastes, in this method has received considerable attention because it is economical and eco-friendly [2]. Batch adsorption studies on the removal of Cr(VI) from aqueous solution using a number of agricultural wastes such as bo tree (*Ficus religiosa*) leaves [1], amla (*Emblica officinalis*) dust [3], sugarcane (*Saccharum fficinarum*) bagasse [4], coconut (*Cocos nucifera*) husk [5], water hyacinth (*Eichhornia crassipes*) [6], and sugar beet (*Beta vulgaris*) bagasse [7] were conducted. Rodriguez *et al*. [8] determined 100% removal of Cr(VI) using *Litchi chinensis sonn* on at optimum conditions i.e. 6 min, at pH 1 and 28 ℃, 5 days incubation, 5 and 10 grams of biomass. The study of Rodriguez [8] was only limited to a batch process and the behaviour of the system in a continuous column process was not evaluated i.e. the effect of varying flow rates, initial sorbate concentration and bed height. This may be due to operational costs involved in actual experimentation by either the batch or the continuous column process. Nowadays, simulations are used to conduct adsorption processes and to predict the effects of varying the adsorption parameters especially advantageous to small and medium industries that could not afford other sophisticated wastewater treatment of heavy metals due to operational costs. The objective of the study is to determine the performance of *Litchi chinensis sonn* in sequestering Cr(VI) in a fixed bed column process by breakthrough curve analysis varying: 1) initial concentration at a constant flow rate and constant bed height, 2) flow rate at constant initial concentration and constant bed height, and 3) bed height at a constant flow rate and constant initial concentration using Aspen Adsorption® V8.4.

Manuscript received May 12, 2019; revised July 4, 2019.

The authors are with the School of Chemical, Biological, and Materials Engineering and Sciences, Mapua University, Muralla St., Intramuros, Manila, 1002, Philippines (e-mail: adnieva@mapua.edu.ph).

II. Materials and Method

A. Batch Adsorption Study

The values for pore space volume, bulk density, power volume, particle density, maximum adsorptive capacity (q_{max}), and isotherm constant b of *Litchi chinensis sonn* were obtained from batch adsorption study where the stock solution of Cr(VI) were prepared using its water-soluble salt form $K_2Cr_2O_7$ as shown in Table I.

TABLE I: Summary of Parameters from Batch Data Needed for Simulation Parameters

Parameter	Value	Unit
q_{max}	0.8972	mg g^{-1}
Isotherm parameter	0.3038	-
Pore space volume	0.0041	ml g^{-1}
Bulk density	0.3741	g cm^{-3}
Pore volume	$4.013x10^{-5}$	cm^3 g
Particle density	$6.23x10^{-1}$	g cm^{-3}

The properties of each biosorbent were analysed using the following laboratory analyses: 1) surface properties using scanning electron microscopy (SEM, Hitachi S-300N), 2) particle size distribution by a laser diffraction particle size analyzer (LSTM 13 320, Beckman, USA), 3) Fourier transform infrared (FTIR, Perkin Elmer Model 1600)

doi: 10.18178/ijesd.2019.10.10.1195

spectroscopy, 4) zeta potential analyzer (ZEN3600, MALVERN Nano-ZS) to determine the surface charges and 5) an elemental analyzer (HORIBA 7021H) to determine the composition in terms of the major elements, 6) Cationic Exchange Capacity (CEC) (Bio-Rex 70) analyzer.

B. Physical and Chemical Properties of Sorbate

The physical and chemical properties of the sorbate, such as electrolyte dissociation reaction, equilibrium constants, and stoichiometry, are readily available at the Aspen Properties®V8.4 software. This software provides the physical properties of these electrolytes in combination with water. The electrolyte used was $K_2Cr_2O_7$, wherein dichromate served as the source of Cr(VI). According to Kutscher et al. [9] and Brandhuber [10], Cr(VI) exists at high pH solutions of at least 5. Thus, to have the presence of Cr(VI) in the stock solution the pH was maintained at high levels. The property method used was ELECNRTL (Electrolyte Non-Random Two Liquid) because it could accommodate whether the system is in high or low concentrations denoting that it is the most flexible electrolyte property method in Aspen Adsorption®. Any liquid electrolyte solution can be handled by this property method unless the vapour phase is associated.

The Non-Random Two-Liquid model calculates liquid activity coefficients and is recommended for highly non-ideal chemical systems for both Vapor-Liquid and Liquid-Liquid equilibrium applications and uses the advanced equation-of-state mixing rules such as Wong Sandler and MHV2 [11] as shown in

$$\begin{aligned} &ln(\gamma_i) \\ &= \frac{\sum_j x_j \tau_{ji} G_{ji}}{\sum_k x_k G_{ji}} \\ &+ \sum_j \frac{x_j G_{ij}}{\sum_k x_k G_{kj}} \left(\tau_{ij} \frac{\sum_m x_m \tau_{mj} G_{mj}}{\sum_k x_k G_{kj}} \right) \end{aligned} \quad (1)$$

where γi is the activity coefficient and the other terms are expressed in

$$G_{ij} = exp\left(-a_{ij}\tau_{ij}\right) \quad (2)$$

$$\tau_{ij} = a_{ij} + \frac{b_{ij}}{T} + e_{ij}\, ln\, T + f_{ij}T \quad (3)$$

$$a_{ij} = c_{ij} + d_{ij}(T - 273.15K) \quad (4)$$

$$\tau_{ij} = 0 \quad (5)$$

$$G_{ij} = 1 \quad (6)$$

where the binary parameters a_{ij}, b_{ij}, c_{ij}, d_{ij}, e_{ij}, f_{ij}, can be determined from VLE and/or LLE data regression. The recommended values for c_{ij} are 0.30 for non-polar substances, 0.20 for saturated hydrocarbons with polar non-associated liquids and systems that exhibit liquid-liquid immiscibility, and 0.47 for strongly self-associated substances with nonpolar substances. With the assumption that the system has no interference with any obstruction, but only dissociation in pure water, the properties of the Cr(VI) was determined using Aspen Properties®V8.4 Electrolytes Wizard [12]. To add the counterion, the component list was saved and converted to a component set. The counter ion was used in able to observe the behavior of a theoretical counter ion during the adsorption process. Based on the biosorbent characterization, the elemental composition of *Litchi chinensis sonn* has 3.48% K^{+1}, which was used as the counterion in the simulation.

C. Feed and Product Block Specification

The process involved consists of an input stream, the adsorption tower, or bed, and the product stream. A sample set-up of the simulation process was shown in Figure 1. For the input stream and output stream configuration, each had a Guide User Interface (GUI) wherein the feed specifications such as the flow rates and the initial sorbate concentration were used as inputs. For the adsorption tower configuration, it also has its own GUI where the parameters for the column and the adsorbents used were provided. In the feed and product blocks, the initial metal concentration, initial counter ion concentration, and flow rates were specified. The anion and the theoretical counterion were the only components in the specification table because water is a default component in Aspen Adsorption® V8.4. The theoretical counterion serves as a tool used to observe the behavior of a certain counter ion for a particular anion during the adsorption process. It will then inform us of how fast the adsorbent saturates and how long can the adsorbent be used before regeneration is needed.

In order to determine the breakthrough time for the adsorption column, the product concentration of Cr(VI) was initially set to zero. The Reversible model was used as the model type of the process. The solvent density, which was water at 25 ℃, was set to 55.41 kmol m^{-3}.

Both the initial and final concentration of the Cr(VI) and counter ion were in terms of equivalence per cubic meter, eq m^{-3}. The initial concentration of Cr(VI) in the feed block was set to be the same with the final concentration of the counter ion and the initial concentration of the counter ion was set to be the same with the final concentration of Cr(VI). Thus, it was assumed that all of the Cr(VI) was adsorbed by the adsorbent. At the feed block, the flow rate of the feed was fixed resulting to a uniform flow rate throughout the adsorption process. This is valid for dilute solutions where the effect of binding ions to the adsorbent is negligible. Upon setting up the adsorption tower as well as the feed and product streams, the feed stream was configured. The density was held constant and the value was assumed to be that of water at 25°C. The initial concentration of the sorbate in the feed was based from trial and error. Most bed configurations would use the default configurations in running the simulation [12].

D. Bed Specification

The simulation of the adsorption process was governed by set of equations that were configured using the tabs i.e. general tab, the material/momentum balance tab, the kinetic model tab, and the isotherm tab at the configure layer form. Under the general tab, the UDS 1 was chosen to be the discretization method for it is a good all-around performer, non-oscillatory in all possible conditions, unconditionally stable, shorter simulation time and has reasonable accuracy.

The Upwind Differencing Scheme 1 is a first-order upwind differencing scheme based on a first order Taylor Expansion [12]. The first-order convection term is shown in

$$\frac{\partial \Gamma_i}{\partial z} = \frac{\Gamma_{i-} \Gamma_{i-1}}{\Delta z} \tag{7}$$

while the second-order dispersion term is represented with a second-order differencing scheme is shown in

$$\frac{\partial^2 \Gamma_i}{\partial z^2} = \frac{\Gamma_{i+1} - 2\Gamma_i + \Gamma_{i-1}}{\Delta z^2} \tag{8}$$

The number of nodes was set to a default of 20 nodes. The overall material balance used by Aspen Adsorption® V8.4 to simulate the ion exchange process is expressed as

$$\upsilon_l \frac{\partial_{pi}}{\partial z} + \varepsilon_i \frac{\partial_{pi}}{\partial t} = 0 \tag{9}$$

where υ_l is the liquid velocity, p_i is the liquid molar density, z is the axial co-ordinate, ε_i is the interparticle voidage, and t is for time. This equation implies that at the extent of the ion exchange process, solvents having different densities are being used in different production, purge and regeneration stages. As a result of the ion exchange process, the density stays the same. The next material balance shown manages the ionic species in the liquid phase fed into the ion-exchange column.

$$-\varepsilon_i E_z \frac{\partial^2 c_k}{\partial z^2} + \upsilon_l \frac{\partial c_k}{\partial z} + \varepsilon_l \frac{\partial c_k}{\partial t} + J_k = 0 \tag{10}$$

where E_z is the axial dispersion coefficient, c_k is the ion concentration in the liquid phase, and J_k is the ion material transfer rate. This ion material transfer rate was measured between the bulk liquid and resin given by (11):

$$J_k = (1 - \varepsilon_i) \frac{\partial w_k}{\partial t} \tag{11}$$

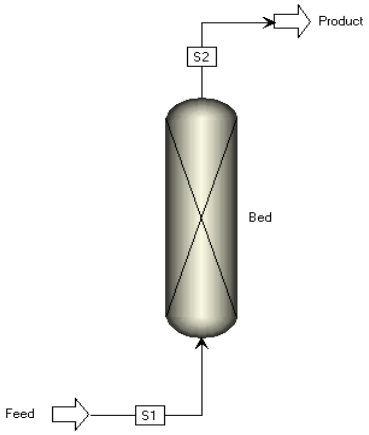

Fig. 1. Sample set-up of the simulation process.

The $\frac{\partial w_k}{\partial t}$ is the uptake rate determined by a solid film linear driving force relationship in

$$\frac{\partial w_k}{\partial t} = MTC_{sk}(w_k^* - w_k) \tag{12}$$

where MTC_{sk} is the solid mass transfer coefficient, w_{k^*} is the ion loading in equilibrium with liquid phase concentration in eq.m^{-3}, and w_k is the ion loading on adsorbent in eq.m^{-3}. The amount of counter ions (K^{+1}) being released from the resin and entering the liquid phase was determined from the amount of ions exchanged from the liquid phase – the total charge of both liquid and resin must remain neutral as shown in

$$J_b = \sum_{k=1\ k\to b}^{nc} J_k \tag{13}$$

where J_b is the counter ion material transfer rate. Thus, the behavior of the exchange counter ion in the liquid phase is represented by the material balance

$$-\varepsilon_i E_z \frac{\partial^2 c_b}{\partial z^2} + \upsilon_l \frac{\partial c_b}{\partial z} + \varepsilon_l \frac{\partial c_b}{\partial t} + \sum_{k=1\ k\to b}^{nc} J_k = 0 \tag{14}$$

where c_b is the counter ion concentration in liquid phase.

In the material/momentum balance tab, the basic assumptions about material dispersion in the liquid phase for ion exchange process are specified. The chosen assumption for the material/momentum balance was convection with estimated dispersion. This assumption includes the dispersion term for the material balance of the bed. The dispersion coefficient changes within the length of the bed and is estimated using the correlation in

$$\frac{\upsilon_i d_p}{E_z} = 0.2 + 0.011 \left(\frac{Re}{\varepsilon_i}\right)^{0.48} \tag{15}$$

where, E_z is the axial dispersion coefficient, υ_i is the liquid velocity, ε_i is the interparticle voidage, d_p is the particle diameter, and Re is the Reynolds number which can be calculated using

$$Re = \frac{\rho_1 M_1 d_p \upsilon_l}{\mu} \tag{16}$$

where μ is the liquid viscosity, ρ_1 is the liquid molar density, and M_1 is the liquid molecular weight.

To determine the overall mass transfer rate, the overall mass transfer of ionic components between the bulk liquid phase and the adsorbed phase must overcome two resistances: 1) mass transfer resistance located in the boundary layer surrounding the particle and 2) mass transfer resistance inside the resin particle. In the case of Aspen Adsorption® V8.4, it has the capability of merging the overall resistance to mass transfer into a one overall factor. The type of mass transfer resistance were selected from: 1) film model assumption, 2) kinetic model assumption, 3) form lumped resistance, and 4) the form of mass transfer coefficient; which were found under the kinetic model tab. Under the film model assumption, the solid film was chosen because the mass transfer driving force is expressed as a function of the solid

phase concentration. The chosen kinetic model assumption was the lumped resistance in linear function because the mass transfer driving force for component k is also expressed as a function of the solid phase concentration. Lastly, under the isotherm tab, the Mass Action Equilibrium was chosen.

E. Missing Parameter Specification and Calculation

Spent The missing parameters can be obtained using different correlations in order to satisfy the adsorption tower specification table. This includes the interparticle voidage (ε_1), intraparticle voidage (ε_p), total resin capacity (Q), and the mass transfer coefficient (MTC) of the metal ions. Given the values of 0.0041, 0.3741, 4.013×10^{-5} and 6.23×10^{1} for pore pace volume, bulk density, power volume and particle density the inter particle voidage and intraparticle voidage of the bed were calculated using

Pore space volume x Bulk Density = Interparticle Voidage (17)

Power Volume x Particle Density = Intraparticle Voidage (18)

The calculated interparticle voidage was 1.5×10^{-3} m^3 m^{-3} and the intraparticle voidage value was 2.50×10^{-3} m^3 m^{-3}. For this monolayer system, the total resin capacity (eq m^{-3}) was calculated using

$$PN_o = \rho q_o (1 - \varepsilon_i) \quad (19)$$

where ρ is the density of the medium at 2300 g m^{-3}, q_o is the maximum capacity of the metal (eq g^{-1}), and ε_i is the intraparticle voidage which is 2.50×10^{-3} m^3 m^{-3}. Solving, the total resin capacity was 8.467 eq m^{-3}. The external mass transfer coefficient of particles in a fixed column was estimated using

$$Sh = 2 + 1.1 Re^{0.6} Sc^{\frac{1}{3}} \quad (20)$$

where $Sh = k_c D_p / D_{AB}$, $Re = D_p u\rho/\mu$, and $Sc = \mu/\rho D_{AB}$. Substituting the definitions of *Sh*, *Re*, and *Sc*, it results to

$$\frac{K_C D_p}{D_{AB}} = 2 + 1.1 \left(\frac{D_p u \rho}{\mu}\right)^{0.6} \left(\frac{\mu}{\rho D_{AB}}\right)^{\frac{1}{3}} \quad (21)$$

where in D_p is the average particle diameter in cm, D_{AB} is the mass diffusivity of solute *A* in solvent *B*, *u* is the fluid velocity in m s^{-1}, ρ is the density of the solution, and μ is the solution viscosity. Since the solution was assumed to be diluted, the fluid bulk density and viscosity were also assumed to be the same as that of water for which values at 25°C were used. At 25°C, water has a density of 997 kg m^{-3} and viscosity of 8.94×10^{-4} kg m^{-1} s^{-1}. D_{AB}, is defined as the mass diffusivity of solute A in solvent B. In aqueous media the electrolytes are dissociated into cations and anions, thus the average mass diffusivity of the electrolyte is a combination of the individual diffusion coefficients of both the cation and anion as shown in

$$D_{AB} = \frac{n_+ + n_-}{\frac{n_-}{D_+} + \frac{n_+}{D_-}} \quad (22)$$

The overall mass diffusivity of the electrolyte $K_2Cr_2O_7$ in water was computed where n^+ is the valence of the cation, n^- is the valence of the anion, and D_i is the diffusion coefficient of the individual ion. The diffusion coefficients of the ions from the dissociated $K_2Cr_2O_7$ electrolyte were D_K+ was computed as 1.96×10^{-7} m^2 s^{-1} and $DCr_20_7^{-2}$ as 1.13×10^{-7} m^2 s^{-1}. The resulting mass diffusivity (D_{AB}) was 1.57×10^{-7} m^2 s^- for Cr(VI). In the adsorption tower, the mass transfer coefficient was set to be constant all throughout the bed. The mass transfer coefficient is a function of fluid velocity that is in relation with the fluid flow rate. Thus, the mass transfer coefficient changed when the flow rate was varied [11]. Table II shows the list of flow rates used along with the corresponding mass transfer coefficient.

TABLE II: MASS TRANSFER COEFFICIENT OF CR(VI) AT DIFFERENT FLOW RATES

Flowrate, L s^{-1}	Kc (Mass Transfer Coefficient), s^{-1}
1.00×10^{-3}	74.0
2.00×10^{-3}	81.1
3.00×10^{-3}	86.9
4.00×10^{-3}	91.9
5.00×10^{-3}	96.5
6.00×10^{-3}	101
7.00×10^{-3}	105
8.00×10^{-3}	108
9.00×10^{-3}	112
10.00×10^{-2}	115

At the process flowsheet window pane, breakthrough flowsheet was added. This flowsheet generated a breakthrough curve that was configured to display concentration diagram of both the Cr(VI) and the corresponding counterion on the product block. The breakthrough plot displayed by Aspen Adsorption® V8.4 is a concentration versus time plot.

F. Simulation

The system was ready to be simulated after the bed configuration and determining all essential parameters. The simulation was started by initializing the process and then shifting to dynamic mode. During the dynamic mode, the breakthrough curve was produced as time progresses. The change in the concentration of Cr(VI) and counter ion was seen in the breakthrough plot window. Over a range of volumetric flow rates (Table II), initial sorbate concentrations and bed heights, several simulations were ran in order to determine the effect of varying each parameter while holding the other parameters constant. To study the effects of varying feed flow rate with respect to the breakthrough time and breakthrough curve of the column, the flow rate was set on ten different values i.e. 20 mg L^{-1}, 40 mg L^{-1}, 60 mg L^{-1}, 80 mg L^{-1}, 100 mg L^{-1}, 120 mg L^{-1}, 140 mg L^{-1}, 160 mg L^{-1}, 180 mg L^{-1}, and 200 mg L^{-1} where the initial sorbate concentration and bed height were held constant. To study the effects of varying initial sorbate concentration with respect to the breakthrough time and breakthrough curve of the column, the initial sorbate concentration was set on the same ten different values where, the feed flow rate and bed height were held constant. To study the effects of varying bed height with respect to the

breakthrough time and breakthrough curve of the column, the initial sorbate concentration was set on three different values: 0.2 m, 0.5 m, and 0.7 m where the feed flow rate and initial sorbate concentration were held constant.

III. Results and Discussions

The simulation of the biosorption of Cr(VI) had a total of 300 runs for the variation of flow rate (10 runs), sorbate concentration (10 runs) and bed height (3 runs). The flow rates used were based on the saturation point of the biosorbent. This was done by trial and error method that indicated that the chosen flow rates were within the range as they produced a successful breakthrough graph since at a flow rate higher than 1.00×10^{-2} L s^{-1}, the breakthrough time was swift and so was the saturation of the biosorbent. In contrast, a flowrate lower than $1.00\text{x}10^{-3}$ L s^{-1} resulted in prolonged breakthrough time than the Aspen Adsorption® software can no longer simulate. In general, a higher or lower amount from the range of values indicated that it would no longer accommodate an efficient adsorption process. Initial sorbate concentrations were 20 mg Ł$^{-1}$ to 200 mg Ł$^{-1}$. The bed heights were based from the mass of the biosorbent used in the batch adsorption study as shown in

$$m_b = \frac{1}{4}\pi D^2 H_b \rho_b \tag{23}$$

where D is the column diameter, H_b is the bed height, and ρ_b is the bulk density of the biosorbent. Also, the range of flow rates, initial sorbate concentrations and bed heights used were based on the capability of the simulation software to produce a breakthrough curve. If the breakthrough plot window was not showing a converged plot of the change in concentrations of the counterion (K^{+1}) and Cr(VI) with respect to time, it only implies that the flow rate, initial sorbate concentration and bed height input are not within the system's adsorption capacity or boundary.

A. Breakthrough Curve Analysis

A longer breakthrough curve time implied better adsorption capacity. This means it would take a longer time for the *Litchi chinensis sonn* to be completely saturated. This was particularly useful as it means that the *Litchi chinensis sonn* could be used for a more extended period before it would need replacement or regeneration. The breakthrough time depended more on flow rate, bed height and particle size, the concentration of the sorbate, solution pH, temperature, and material properties. After the breakthrough time, the adsorption capacity of adsorbent reduced abruptly.

Results indicate that increasing the initial sorbate concentration had a slight effect on breakthrough time; the breakthrough time decreased at an average value of 1.5147 s. However, increasing the initial concentration affected the amount by which equilibrium breakthrough concentration was achieved by half the amount of total sorbate concentration. Decreasing the amount of Cr(VI) increased its contact time with the biosorbent. The slower breakthrough time under the lower concentration of Cr(VI) showed the importance of intra-particle diffusion in the adsorption process. Intra-particle diffusion is a process involving the movement of species from the bulk of the solution to the solid phase. This mechanism describes a well-stirred batch adsorption system.

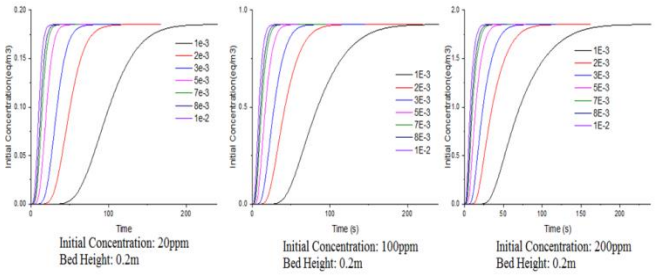

Fig. 2. Comparison of the breakthrough curves of constant flowrate, constant bed height, and varying initial concentration.

B. Varying Initial Sorbate Concentration at Constant Bed Height and Flow Rate

The effect of the initial concentration towards the system was determined by varying the initial concentration from 20 mg L^{-1} to 200 mg L^{-1} at constant bed height and constant flow rate. Figure 2 shows the breakthrough curves for a column system having a bed height of 0.2 m and flow rates from 1.00×10^{-3} L s^{-1} to 1.00×10^{-2} L s^{-1} with varying initial concentration of 20 mg Ł$^{-1}$, 100 mg Ł$^{-1}$, and 200 mg Ł$^{-1}$, respectively.

By observing one constant flow rate, at high initial concentration the breakthrough curves are steeper. On the other hand, at low initial concentration the breakthrough curves lose its steepness. Generally, a breakthrough curve describes the extent to which the capacity of an adsorbent bed was utilized. A steeper breakthrough curve indicates that the column saturates faster during the adsorption process. While, a less steep breakthrough curve implies low saturation of the column at a low initial metal concentration as there are fewer metal ions present in the solution. The SEM analysis results shown in Fig. 3 indicates that *Litchi chinensis sonn* peels have high porosity due to its rough surface that served as the binding sites for the sorbate. Faster clogging of these pores occurred when the amount of sorbate flowing through the column was increased.

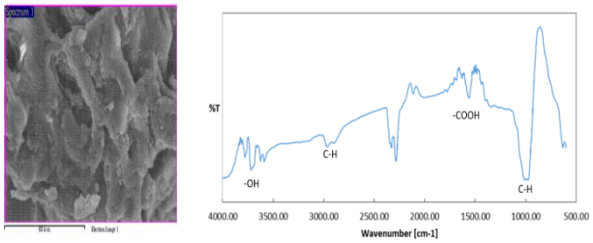

Fig. 3. SEM (left) and FTIR (right) result of *Litchi chinensis sonn* peels.

The way that the adsorbent bed capacity was utilized is supported by the possible reaction mechanism of the adsorption process which is ion exchange. The matrix of a *Litchi chinensis sonn* peel is composed of a hydroxyl carboxyl group (R) specifically 3726.76 cm^{-1} for –OH, 2900 cm^{-1} for C–H, 1536.99 cm^{-1} for –COO, 1185.04 cm^{-1} for C–OH, and 853.34 cm^{-1} for C–H capable of binding with any positively charged ions of the sorbate as shown in FTIR results in Fig. 3 and the K^{+1} counterion (B). As Cr(VI) ions

were exposed through the surface of the biosorbent matrix, an exchange reaction happened between the K^+ counterion and the Cr(VI) ions. The K^{+1} were removed from the matrix through electrostatic interaction and the Cr(VI) ions would then bind into the slots were the K^{+1} stayed.

Elemental analysis shows that 3.48% of K^{+1} and 0.53% of Mg^{+2} were present on the surface of *Litchi chinensis sonn*. Comparing the percent composition of Mg^{+2} and K^{+1}, there is a 6.57 unit of K^{+1} per 1 unit of Mg^{+2}. Since Aspen Adsorption V8.4 is incapable of dealing with dual counterions, it was assumed that the adsorption of Cr(VI) favoured that of the K^{+1} since there was a higher amount present. The claims were verified upon comparing the physical properties of the counterions with that of Cr(VI) (i.e., ionic radius and electronegativity). According to the law of electronegativity, the power of an atom in a molecule to attract electrons by itself is greater as the difference between electronegativity increases. The difference between the electronegativity of K^{+1} and Cr(VI) is 0.84 while the difference between the electronegativity of Mg^{+2} and Cr(VI) is 0.35. Since K^{+1} and Cr(VI) has higher electronegativity difference as compared to Mg^{+2} and Cr(VI), Cr(VI) had greater attraction. Comparing also the ionic radius, it was obvious that K^{+1} could accommodate more Cr(VI) since it has a higher ionic radius than that of Mg^{+2}.

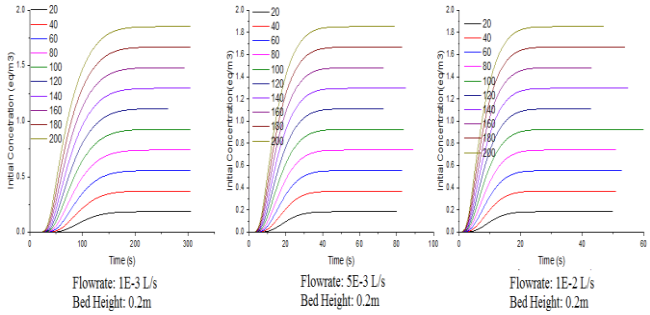

Fig. 4. Comparison of the breakthrough curves of constant initial sorbate concentration, constant bed height, and varying flow rate.

C. Varying Flow Rate at Constant Initial Sorbate and Bed Height

The flow rates used were varied from 1.00×10^{-3} L s^{-1} to 1.00×10^{2} L s^{-1} and the breakthrough curves for a column system having a bed height of 0.2 m and initial concentration from 20 mg $Ł^{-1}$ to 200 mg $Ł^{-1}$ were shown in Fig. 4. By observing one constant initial concentration, it can be seen that increasing the flowrate resulted to a steeper breakthrough curve. Although SEM results showed high porosity of the biosorbent, but faster clogging of the biosorbent pores occurred due to the increased movement of the fluid as the velocity of sorbate entering the pores of the sorbent also increased. According to Ansari *et al*. [13], the biosorbent saturated faster since there was a large amount of Cr(VI) entering its pores. Decreasing the amount of Cr(VI) increased its contact time with the biosorbent and would result in higher removal of Cr(VI) in the column.

Varying the flow rate had the same effect with the breakthrough concentration in varying the initial concentration. The equilibrium breakthrough concentration was achieved by half the amount of total sorbate concentration. The breakthrough time decreased at an average value of 12.244 seconds, indicating that an increase in flow rate decreased the breakthrough time. As the solution flows through the bed column, axial dispersion or mixing may happen. If in case mixing occurs, the efficiency of the bed in removing the metal ions is reduced. To check whether axial dispersion is significant or not the equation below was used.

$$\frac{\partial w_k}{\partial t} = MTC_{sk}(w_k^* - w_k) \tag{24}$$

where d is bed diameter, v is the volumetric flow rate, ρ is the liquid density, μ is liquid viscosity, and D is diffusivity. The bed diameter, liquid density, liquid viscosity, and diffusivity are constant while volumetric flow rate varies. Peclet number (Pe) measures the degree of dispersion introduced into the system. If Pe is less than 30, axial dispersion is substantial; if it is greater than 100, the bed operates under near plug flow conditions; and if the value is going towards positive infinity, the bed operates under plug flow condition. The calculation of Peclet number in all considered flow rates in the study leads to similar results, wherein the values were going towards positive infinity. Thus, the axial dispersion is not significant in the system due to the bed was operating under plug flow condition [11].

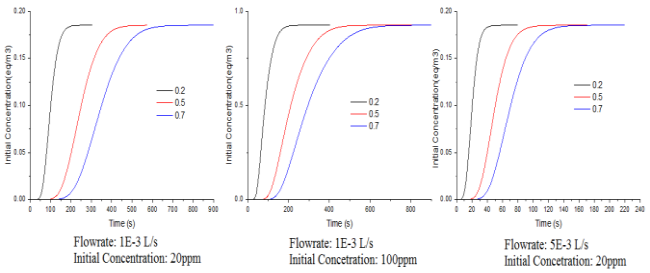

Fig. 5. Comparison of the breakthrough curves of constant flow rate, constant initial concentration, and varying bed height.

D. Varying Bed Height at Constant Flow Rate and Initial Sorbate

Fig. 5 shows the breakthrough curves for a column system having flow rates of 1.00×10^{-3} L s^{-1} to 5.00×10^{-3} L s^{-1} and initial concentration from 20 mg $Ł^{-1}$ to 100 mg $Ł^{-1}$ with varying bed height of 0.2 m, 0.5 m, and 0.7 m respectively. Results show that with increasing bed height, the breakthrough curve became steeper. The breakthrough time increased as the bed height increases, with that there was a higher removal efficiency of Cr(VI) because Cr(VI) had more time to get in contact with the biosorbent. A higher bed height would provide more binding sites for the sorption resulting in an increase in breakthrough time; thus, a higher removal of contaminant would be observed. A lower bed height implies a smaller capacity of the bed to adsorb metal ions from the solution and thus resulting in a faster breakthrough time. Also, in lower bed heights, axial dispersion is considered as the predominant mass transfer phenomenon which reduces the diffusion of metal ions [14]. As observed from each figure, increasing the initial sorbate concentration increased adsorptive capacity, q_{eq} and resulted in a faster equilibrium time, same with increasing flowrate. This was the reverse of increasing bed height, as increasing

the bed height resulted in a slower breakthrough time and an increase in q_{eq}.

IV. Conclusions

The performance of *Litchi chinensis sonn* peels towards sequestration of Cr(VI) in a fixed bed column was investigated through breakthrough curve analysis by variation of the initial sorbate concentration, volumetric flow rate or column bed height. A good adsorption capacity was implied by a longer breakthrough time. The breakthrough time depended more on flow rate, bed height and particle size, concentration of pollutant, solution pH, and material properties. Increasing the initial sorbate concentration and volumetric flow rate resulted to a faster breakthrough time since the biosorbent saturated faster since there was a decrease in contact time. The reverse could happen when increasing the bed height, as it resulted to more binding sites for adsorption to occur, thus slower breakthrough time. The slowest breakthrough time was 335 s with volumetric flowrate at $1x10^{-3}$ L s^{-1}, initial sorbate concentration at 20 mg L^{-1}, and a bed height of 0.7 m. While, the fastest breakthrough time was 6.63 s with volumetric flow rate at $1x10^{-2}$ L s^{-1}, initial sorbate concentration at 200 mg L^{-1}, and bed height of 0.2 m.

Conflict of Interest

The authors declare no conflict of interest.

Author Contributions

A facilitated the whole research process and write-ups construction; *B, C* conducted the research, analyzed the data, and wrote the paper; all authors approved the final revision of the paper.

References

[1] R. Gayathri, M. Thirumarimurugan, and T. Kannadasan, *Der Chemica Sinica*, vol. 4, pp. 79-80, 2014.
[2] M. Šćiban, J. Prodanović, and R. Razmovski, *Acta Period. Technol.*, vol. 43, p. 335, 2014.
[3] K. Anbalagan and J. Juliet, *Indian Journal of Chemistry*, vol. 43, pp. 45-50, 2004.
[4] K. Bahadur and M. Paramatma, *Research Journal of Chemical Sciences*, vol. 4, pp. 32-33, 2014.
[5] O. Olayinka, O. Oyedeji, and A. Oyeyiola, *Afr. J. Environ. Sci. Technol.*, pp. 286-287, 2009.
[6] S. Hansan, D. Ranjan, and M. Talat, *Bioresources*, vol. 5, pp. 563-565, 2010.
[7] M. Samadi, A. Rahman, M. Zarrabi, E. Shahabi, and F. Sameei, *Environ. Technol.*, vol. 30, pp. 1023-1029, 2009.
[8] I. Rodriguez, R. Perez, J. Gonzales, M. Zarate, and V. Juarez, *American Journal of Biochemistry and Biotechnology*, pp. 7-13, 2012.
[9] D. Kutscher, S. McSheehy, and J. Wills, Thermo Fischer Scientific Inc, 2012.
[10] P. Brandhuber, C. Seidel, N. Blute, Y. Wu, B. Alspach, and I. Najm, *Water Research Foundation*, 2005.
[11] H. Fogler and N. Gurmen, *Aspen PlisTM Workshop for Reaction Engineering and Design*, 2002.
[12] *Aspen Technology Incorporated (ATI)*, 2010.
[13] R. Ansari, B. Seyghali, I. Mohammad-khah, and M. Ali, *J. Surfactants Deterg.*, vol. 15, pp. 557-560, 2012.
[14] S. Singha, U. Sarkar, S. Mondal, and S. Saha, *Desalination*, vol. 279, pp. 48-58, 2012.

Aileen D. Nieva is the current director of the Mapua University Center for Continuing Education and Special Competencies. She graduated from Mapua University (formerly Mapua Institute of Technology) with a Ph.D. of chemical engineering.

Dr. Nieva has an immense amount of experience and training in technical consultancy and auditing jobs, specializing in waterworks and environmental sector. She is an environmental consultant, registered chemical engineer, certified QMS auditor, and lead auditor for ISO 9001:2008.

She is a professor at Mapua University since 1995 in environmental engineering, chemical engineering, differential equations, air pollution control, and specializing track such as Sustainable Engineering Technology. She received various awards such as Magna Cum Laude (Master of Science in Chemical Engineering), Most Outstanding Faculty Member 2002 (School of Chemical Engineering and Chemistry), and more.